FINAL TECHNICAL REPORT

FOR
NCC 3 211

ON LINE QUANTIFICATION OF CRYSTAL SURFACES BY STEREO IMAGING

SUBMITTED BY
CELAL BATUR
DEPARTMENT OF MECHANICAL ENGINEERING
THE UNIVERSITY OF AKRON
AKRON OHIO 44325-3903

SUBMITTED TO
NASA LEWIS RESEARCH CENTER
GRANTS OFFICER,
MAIL STOP 500-315
21000 BROOKPARK ROAD
CLEVELAND OHIO 44135

WALTER M. B. DUVAL
PROCESSING SCIENCE AND TECHNOLOGY BRANCH
MAIL STOP 105-1
21000 BROOKPARK ROAD
CLEVELAND OHIO 44135

NASA SCIENTIFIC AND TECHNOLOGY FACILITY
P.O. BOX 8757
BWI AIRPORT
MD 21240

OFFICE OF NAVAL RESEARCH
RESIDENT REPRESENTATIVE
1960 KENNY ROAD
COLUMBUS OH 42310-1063

APPLICATION OF STEREO IMAGING FOR RECOGNITION OF CRYSTAL SURFACE SHAPES

C. Batur
Department of Mechanical Engineering
The University of Akron
Akron, Ohio 44325-3903

ABSTRACT

The shape of an interface while a crystal is growing inside a crystal growth furnace is an important measurement to assess the crystal quality on-line. If the crystal surface can be visualized by video or x-ray imaging, the interface shape can be determined by the stereo image processing techniques. This paper presents a methodology to determine the shape of the solid-melt interface by stereo based imaging techniques while the crystal is growing inside a transparent furnace. The methodology generates a qualitative shape information provided that a good pair of stereo images of the interface can be captured. For a quantitative shape description, i.e., for the determination of interface points with respect to a fixed coordinate frame, both cameras must be calibrated. This paper illustrates the methodology for qualitative shape determination of Lead Bromide crystal interface.

1. INTRODUCTION

The shape of an interface between the solid and liquid phases is one measurement that immediately describes how the crystal is growing. Although it is not exactly known how the interface shape is related to crystal quality, nevertheless, it is commonly accepted that crystals which grow with a flat interface have better structural properties. The basic reason behind this assumption is the fact that, if the interface is flat, thermal stresses inside

the material are at minimum levels, **[Chang and Wilcox, 1974]**. Furthermore, crystalline imperfections are also at a minimum level within a flat growing interface. Therefore, on-line measurement of the interface shape is important for crystal growth control.

The interface shape is determined by the furnace dynamics, the material properties and the geometry of the ampoule that encapsulates the material. The furnace that we consider in this paper is the vertical Bridgman type as shown in **Figure 1** and the material is Lead Bromide ($PbBr_2$). Basically, there are two inputs that a process operator can manipulate to control the growth process: the axial temperature profile within the furnace and the translational speed of the ampoule **[Singh et al 1988]**. Simulation studies recommend specific temperature profiles that will generate a flat interface in the steady state, **[Taghavi and Duval, 1989], [Dantzig and Tortorelli 1991]**. In this paper, we propose a stereo based imaging technique that can verify these theoretical findings by providing three-dimensional interface shape information.

The interface quantification by mono image processing techniques is first demonstrated on the Czochralski growth of silver by **[Bachman et al, 1970]**. They used a video signal to determine the diameter of the crystal at the interface. **[Archibald et al, 1988, 1991] , [Kakimoto et al 1988]** worked with x-ray based images to locate the position of the interface. Their procedure works on the intensity difference of x-ray signals that are transmitted through the solid and the melt. **[Wargo and Witt, 1992]** developed a thermal imaging system for the analysis of melt surface thermal field distributions in the Czochralski furnace. **[Batur et al, 1992]** applied the Hueckel edge detection algorithm to a mono video image and determined the shape of interface. Conceptually, this methodology can determine the three dimensional shape by rotating the camera around the interface and repeating the mono image processing algorithm on images coming from different viewing angles.

Our motivation in this paper is to provide three-dimensional solid-melt interface shape information by stereo image processing techniques while the crystal is growing

inside a transparent furnace. If the furnace is not transparent, we assume that x-ray or ultrasound imaging can provide a pair of stereo images for interface quantification. The basic use of the shape information is to establish a dynamic model that correlates the effects of the axial temperature profile and the ampoule's translational speed on the shape of the interface. The dynamic relation between the temperature profile, the translational speed and the resulting interface shape can be used for the design of interface controller.

This paper is organized as follows. In Section 2 we explain the stereo imaging procedure used. The selection of surface points for which the matching is accomplished is described in Section 2.1. The matching procedure is given in Section 2.2. The sources of experimental and theoretical errors are listed and discussed in Section 3. Section 4 presents an application on the Lead Bromide crystal. Finally, conclusions are stated in Section 5 .

2. THE STEREO IMAGING PROCEDURE

The stereo imaging task involves the perception of depth from a pair of two-dimensional images. **Figure 2** describes how this task can be accomplished. A point on the melt-solid interface is denoted as P(X,Y,Z). If we assume a pin hole type lens for both cameras, then the object point P(X,Y,Z), appears as point $P_L(x,y)$ on the left image and as point $P_R(x,y)$ on the right image. The capital letters are used to indicate the position of point P with respect to an absolute coordinate frame (X,Y,Z). The lower case characters, (x,y), define the position of the images of object point P in terms of image plane coordinates. Since we do not know where the object point P is, we first have to find image points that correspond to the same object point as in the case of points P_L and P_R. This is commonly known as the matching problem. Once the matching problem is solved, determination of the depth information can be accomplished in two different ways.

1. If the location of focal points FP_L and FP_R are known, then, intersecting lines (P_L-FP_L) and (P_R-FP_R) gives the location of the object point P. However, for most

practical cases, the camera focal point is not exactly known, or, there may not be a single, pin-hole type focal point. For these cases, it is necessary to calibrate the cameras. The camera calibration equations define a focal point in a least squares sense **[Martins et al 1981]**.

2. If only qualitative interface shape information is needed, the camera calibration procedure can be avoided altogether. Assuming that two identical cameras are operated at the same magnification level and are placed on the same plane, the images of point P are at the same height as shown in **Figure 2**. The disparity, i.e., the difference in x-coordinates, is proportional to the distance between the cameras and the object point. Following the view from the top, as given **Figure 3**, the relation between the disparity and the depth can be expressed as

$$d = \text{depth} = 2\ e\ f / (x_R + x_L) \qquad 2.1$$

Where (2e) is the distance between the optical axes of cameras, f is the common focal distance, x_R and x_L are the coordinates of the image points in the right and the left image planes, respectively. The disparity is given by $(x_R + x_L)$. The measurement of disparity provides a value that is directly proportional to the depth. This is a simple technique because it does not require camera calibration. However, the disadvantage is that it can provide measurements that are only proportional to depth of interface points. Furthermore, cameras should be identical and be mounted on the same plane. Since the main motivation of our study is to quantify the shape of the interface as flat, convex or concave, we decided to use this second technique.

The stereo imaging methodology basically implements:

(a) the extraction of feature points to be matched such as $P_L(x,y)$ and $P_R(x,y)$ in the images, and

(b) the matching of the feature points so that we can determine that both $P_L(x,y)$ and $P_R(x,y)$ belong to the same object point P(X,Y,Z).

We discuss the feature extraction problem in Section 2.1 and describe the stereo matching procedure in Section 2.2 .

2.1 SELECTION OF INTERFACE POINTS TO BE MATCHED

It is computationally prohibitive to match every point in the left image to every corresponding point in the right image. It is much more efficient to pick points that have certain characteristic features and use them in the matching procedure. The characteristic points that are used in this paper are the edge points in images. The location of edge points are determined by convolving the image with a Laplacian of Gaussian (LOG) filter. The LOG filter is a two-dimensional operator given by,

$$G(x,y) = \sigma^2 \exp\frac{-(x^2+y^2)}{2\sigma} \qquad (2.1.1)$$

Where (x,y) is the location where the filter operates, G(x,y) is the gray level of the image pixel at (x,y) and σ is the variance of the filter. **Figure 4** shows qualitatively the effect of the LOG filter on a one-dimensional edge. The location of edge point is determined by the location of the zero crossing. The zero crossing is the point where the convolved image changes the sign of its image intensity. The LOG filter is obtained by taking the Laplacian of a Gaussian filter. The filter determines the second derivative of the image at point (x,y). However, since the derivative operator amplifies the noise, we filter the image by a low pass Gaussian type smoothing filter before we determine the second derivative of the image. The parameter σ determines how much smoothing is applied. **Figure 5** shows the shape of a typical filter and the derivation of (2.1.1) is given in Appendix A. The LOG filter has a value of zero at the edge of its tail and has a negative central region. The

diameter of the negative central region, w_{2D} is proportional to σ and is given by, **(Grimson, 1981)**.

$$w_{2D} = 2\sqrt{2}\sigma \qquad (2.1.2)$$

The effect of changing w_{2D} is the change in the amount of low pass filtering that is applied to the image. Therefore, w_{2D} adjusts the sensitivity of the LOG filter to image noise. The actual implementation of the continuos LOG filter, (2.1.1), is performed by discretizing the filter and applying it to the image at each pixel location (x,y).. We normalize the discrete filter such that the volume occupied by the negative region of the filter equals to the volume occupied by the positive side of the filter. This modification assures that if there is no edge, the output of the filter is zero.

The edge points or equivalently zero crossings of an image are detected by scanning the LOG filtered image horizontally from left to right. The locations where the filtered image intensity switches sign are marked as location of edges. Once the edge points of both the left and the right images are detected, the final step involves the matching of edge points of the left image to the edge points of the right image.

2.2 MATCHING PROCEDURE

Figure 6 illustrates the matching procedure for a pair of a stereo image. It shows the LOG profiles, i.e., the LOG image intensities that are obtained from a horizontal scan in both the left and the right images. The matching procedure makes use of the LOG profile around a zero crossing point. We consider the left LOG profile around a zero crossing within a window and match this profile to the one inside a sliding window in the right LOG image. Effectively, we compare a LOG pattern around a zero crossing on the left image to another LOG pattern around a zero crossing on the right image. If they are

similar according to a given index, we assume that zero crossing points match. The matching index (MI) is defined as follows

$$MI = \sum_{k=-10}^{k=10} \left| G_l(x_l^* + k, y_l^*) - G_r(x_r^* + k, y_r^*) \right| \qquad k \neq 0 \tag{2.2.1}$$

Where (x_l^*, y_l^*) and (x_r^*, y_r^*) are the coordinates of zero crossing points in left and right images, respectively. This measure compares a total of 20 values of the LOG image intensities at the row position $y_l^* = y_r^*$. If the matching index is found smaller then a specified threshold, then the point (x_l^*, y_l^*) is assumed to match the point (x_r^*, y_r^*).

If the image is noisy, certain zero crossings of the LOG filter are generated due noise. To minimize the effect of noise, a user defined threshold band is used to eliminate noise induced zero crossings. If the neighboring pixels to the zero crossing points of the LOG profile lie within the threshold band, then, that zero crossing is treated as noise and not considered for matching . For example, the zero crossing point ZC on the left LOG profile of Fig. 6 is not considered for matching because it remains within the threshold band. The threshold band and the size of window are tunable parameters that can be altered to improve the stereo matching algorithm. The stereo matching procedure is summarized by the following steps.

1. Convolve both left and right images with a LOG filter of (2.1.1).
2. Scan the left convolved image horizontally from left to right and determine zero crossings.
3. Scan the right convolved image horizontally from left to right and determine zero crossings.
4. Eliminate all zero crossings that are considered to be generated by noise.
5. Compare the zero crossing profiles in the left and right windows by the MI index of (2.2.1).

6. If both profiles are the same, then label the pixels that correspond to left and right zero crossings as a matched points.
7. Repeat steps 2-7 over the entire image.
8. Determine disparities at matched points by (2.1).

3. ERROR ANALYSIS

Since our methodology first finds the edge points and then matches them for stereo quantification, we should consider possible error sources for each step.

A. Errors in Edge Detection.

A1. Shift in Perceived Edge Locations

The zero crossings obtained from the LOG filtered image do not exactly correspond to the actual edge locations. This is illustrated in **Figure** 7 where two different LOG filters are operating on an image of 10 pixels wide. The first filter, shown in Fig. 7a, has $w_{2D} = 11$ and the second filter has a wider band as $w_{2D} = 17$. It can be seen that the actual edge locations and the zero crossings are at significantly different locations in the second case. The shift in the edge location depends on the width of the LOG filter and increases with the increase in w_{2D}. Obviously, if there is no need to low pass filter the image, then there will be a minimal shift since the LOG filter simply becomes a Laplacian filter. However, this is seldom the case in practice. To demonstrate a two-dimensional case, we illustrate the distortions generated by two different filters on the edges of a small gray square as shown in **Figure 8**. From left to right, Fig. 8a shows the original image, the LOG image and the zero crossings, based on $w_{2D} = 11$. The LOG image in the center is normalized to a gray tone range of 0 - 63 for illustration. In Fig. 8b, the LOG filter has a wider bandwidth, $w_{2D} = 17$, therefore, it causes a significant distortion on the edges.

It is difficult to quantify the amount of distortion since it depends on the shape of the edge and gray tone levels of the picture surrounded by the edge. We assume the distortion does not significantly effect our results. This assumption is justified by the following facts:

(a) The same LOG filter is used for both the left and right image,

(b) The left and right images are not significantly different views of the interface, i.e., the disparity in our stereo images is small and finally

(c) we are only interested in obtaining a qualitative shape information for the crystal growth interface.

A2. Non-identical Cameras

Our methodology assumes that two identical cameras are used to obtain the left and right images. Therefore, the focal lenses, the gains and the lens openings of cameras are expected to be identical. It is difficult to realize this configuration in practice. The lack of identical cameras introduces varying light intensities and magnifications for the same viewing area and therefore adversely affects the LOG filtered images. To avoid the error due to non-identical cameras, we used only one camera and obtained both the left and the right image by sliding the camera sideways on the mounting table. Since the crystal growth is a slow process, the shape of the interface does not change significantly during the time that the camera is repositioned .

B. Errors in Matching

A zero crossing point on the left image is a matching point to a zero crossing point on the right image if the LOG values around the zero crossings on the left and right images are similar. The zero crossing points are matched by comparing the LOG patterns around these points. The pattern is defined by the LOG values within a user specified window. A small window may not be sufficient to characterize the pattern, therefore, matching points may be missed. On the other hand, a large window requires excessive computation. A practical window size is determined as a compromise between these two effects.

The second problem is the false matches which are caused by zero crossings due to image noise. The typical characteristics of these zero crossings are small LOG magnitudes around zero crossing points. We define a threshold band to ignore these noise induced

zero crossings, c.f. **Fig. 6**. The effect of using a large threshold band is the loss of potential matching points. On the other hand, if the threshold band width is made too narrow, the algorithm may generate too many false matches. Some of these false matches can be eliminated later if the maximum disparity within the image is known apriori. Again, a practical threshold band is determined as a compromise between missing a matched pair or generating a false match.

4. APPLICATIONS

We present two applications of the stereo imaging procedure to quantify the shape of the solid-melt surfaces for Lead Bromide crystals. These crystals are mainly used as acousto-optic tunable filters, see for example, **[Singh et al 1992a, 1992b]**. **Figures 9a and 9b** are the left and right camera views of the interface. The cameras are looking at the interface with an azimuth angle of 45 degrees. Figures 9e and 9f show the location of zero crossings, i.e., the perceived edge points of the crystal surface. These figures are obtained by determining the zero crossing points on the LOG images Figs. 9c and 9d. Since the LOG images have positive and negative values, for the purpose of presentation, the pixel gray tones in Figs 9c and 9d are scaled such that all gray tones are between 0 and 63. An optimum LOG filter size, w_{2D}, is searched by a trial and error procedure and $w_{2D} = 11$ is found sufficient. The matching edge points are obtained by following the matching algorithm of Section 3.2. The threshold value used for the matching index (MI) is ten. To avoid zero crossing points due to noise, a threshold band of four pixels is used, c.f. Fig. 6. Finally, using (3.1), the disparities at matching points are determined and presented in **Fig. 10a**. There are two options to present the disparities. Here, we used the left image and plotted the disparities at matched points of the left image. The other equally valid alternative is to plot the disparities at the matched points of the right image. Since the disparity is proportional to depth, Fig. 10a essentially displays the reconstructed three-dimensional shape of the interface. In Fig. 10b we present a complete view of the

ampoule. A small box placed on the figure shows the location where the original left and right views are obtained. By looking at the marked region, a human eye sees the crystal surface very similar to the one represented by the disparity profile of Fig. 10a.

For the second application, cameras are positioned to capture the cylindrical side view of the crystal . **Figs. 11a and 11b** show the left and right camera images. A LOG filter with $w_{2D} = 11$ is applied to both images. The LOG filtered images are again scaled in their gray tones to a range of 0-63 and shown in Fig. 11c and 11d, respectively. The zero crossings are illustrated in Figs. 11e and 11f. The edge points are matched with a matching index threshold value of ten. The same noise threshold band of four pixels is used to eliminate the noise induced zero crossings. The disparities of matching points are determined and plotted on the left image as shown in **Fig.12.** This is the three-dimensional interpretation of the actual shape of the crystal. The shape is very similar to what human eyes would see.

5. CONCLUSION

The shape of a melt-solid interface of crystal can be determined by stereo image processing techniques. The methodology presented in this paper first finds the edge points that represent the interface in images and matches the edge points to determine the disparity. Because of the placement of cameras, the disparity is proportional to depth, therefore, a qualitative shape information for the interface can be directly obtained from the plot of disparities. If the cameras are calibrated, i.e., the focal points and image plane locations are exactly known then the interface shape can be determined quantitatively. Since the basic motivation here is to describe the shape as flat, convex or concave, the quantitative shape determination is not explored in this paper. However, extension to quantitative stereo imaging is straightforward.

The technique requires apriori selection of a set of parameters that controls the acquisition of the interface shape information. The effects of these parameters on the determination of the interface shape are discussed in the paper.

Two applications of the methodology on the Lead Bromide crystal are presented. In each case, the three-dimensional shape information is reconstructed successfully from a pair of stereo images.

REFERENCES

1. Archibald L.F., Debnam J.W., Berry F.R., " Imaging of Directional Solidification Interfaces", NASA Technical Briefs., February 1988.

2. Archibald L.F., Debnam J., Berry R.F., Simchick S.K., Sorokach S.K., Barber P.G., "Characterization of the Bridgman Crystal Growth Process by Radiographic Imaging", International Symposium on Optical Applied Science and Engineering July 21-26, 1991 San Diego, Cal., Paper # 1557-35.

3. Bachman K.J., Kirsh H.J., " Programmed Czochralski Growth of Metals" Journal of Crystal Growth, Vol. 7 p.290-295, 1970.

4. Batur C., Sharpless R.B., Duval W.M.B., Rosenthal B.N., Singh N.B., " Identification and Control of a Multizone Crystal Growth Furnace" ,Journal of Crystal Growth, 119 pp: 371-380, 1992.

5. Chang E.C,. Wilcox R.W., "Control of Interface in the Vertical Bridgman-Sockbarger Technique ", Journal of Crystal Growth, Vol. 21 , pp.135-140, 1974

6. Dantzig J.A., Tortorelli D.A., " Optimal Design of Solidification Processes", In Conference on Inverse Design Concepts and Optimization in Engineering Sciences III (Proceedings ICIDES-III), pages 213-226, Washington, DC, Oct. 23-25, 1991.

7. Grimson, William Eric Leifur, "From Images To Surfaces", The MIT Press, 1981.

8. Kakimoto K., Eguchi M., Watanabe H., Hibiya T., " In-situ Observation of Solid-Liquid Interface Shape by X-Ray Radiography During Silicon Single Crystal Growth", Journal of Crystal Growth, 91, 509-514, 1988.

9. Martins H.A., Birk J.R., Kelly R.B., "Camera Models Based on Data from two Calibration Planes," Computer Vision, Graphics and Image Processing, Vol. 17, 1981, pp. 173-180.

10. Singh N.B., Duval W.M.B., Rosenthal B.N. "Directionally Solidified Lead Chloride" Journal of Crystal Growth, 89., pp. 80 , 1988

11. Singh N.B., Gottlieb M., Henningsten R.H., Hopkins R., Mazelksy R., Glicksman M.E., Coriell S.R., Santaro G.J., Duval W.M.B., " Growth and Characterization of Lead Bromide Crystalsa " Journal f Crystal Growth, 123, pp. 221-226, 1992.

12. Singh N.B., Gottlieb M., Henningsten R.H., Hopkins R., Mazelksy R., Glicksman M.E., Coriell S.R., Duval W.M.B., Santaro G.J.," Effect of Growth Conditions on the Quality of Lead Bromide Crystals" , Journal of Crystal Growth, 112, pp. 227-235, 1992.

13. Taghavi K., Duval W.M.B, "Inverse Heat Transfer Analysis of Bridgman Crystal Growth", International Journal of Heat and Mass Transfer. Vol 32, No. 9 pp. 1741-1750, 1989.

14. Wargo M.J., Witt A.F., "Real Time Thermal Imaging for Analysis and Control of Crystal Growth by the Czochralski Technique", Journal of Crystal Growth, Vol. 116 , pp.213-224, 1992

APPENDIX A

Derivation of the Laplacian of Gaussian (LOG) operator

The governing 2-dimensional Gaussian function is given by the following equation,

$$G(x,y) = \sigma^2 \exp\left(\frac{-(x^2+y^2)}{2\,\sigma}\right) \qquad \text{A-1}$$

The Laplacian of $G(x,y)$ is given by,

$$\nabla^2 G(x,y) = \frac{\partial^2 G(x,y)}{\partial x^2} + \frac{\partial^2 G(x,y)}{\partial y^2} \qquad \text{A-2}$$

The first partial derivative of $G(x,y)$ with respect to x can be written as,

$$\frac{\partial G(x,y)}{\partial x} = \sigma^2 \left(\frac{-2\,x}{2\,\sigma^2}\right) \exp\left(\frac{-(x^2+y^2)}{2\,\sigma^2}\right) = -x \exp\left(\frac{-(x^2+y^2)}{2\,\sigma^2}\right) \qquad \text{A-3}$$

The second partial derivative of $G(x,y)$ with respect to x can be written as,

$$\frac{\partial^2 G(x,y)}{\partial x^2} = -\exp\left(\frac{-(x^2+y^2)}{2\,\sigma^2}\right) - x\left(\frac{-2\,x}{2\,\sigma^2}\right)\exp\left(\frac{-(x^2+y^2)}{2\,\sigma^2}\right) = \left(\frac{x^2}{\sigma^2} - 1\right)\exp\left(\frac{-(x^2+y^2)}{2\,\sigma^2}\right) \qquad \text{A-4}$$

Similarly, the second partial derivative of $G(x,y)$ with respect to y can be written as,

$$\frac{\partial^2 G(x,y)}{\partial y^2} = \left(\frac{y^2}{\sigma^2} - 1\right)\exp\left(\frac{-(x^2+y^2)}{2\,\sigma^2}\right) \qquad \text{A-5}$$

Combining equations A-4 and A-5 , the Laplacian of Gaussian operator can be written as,

$$\nabla^2 G(x,y) = \left(\frac{(x^2+y^2) - 2\,\sigma^2}{\sigma^2} \right) \exp\left(\frac{-(x^2+y^2)}{2\,\sigma^2} \right) \qquad \text{A-6}$$

Defining $r = \sqrt{x^2+y^2}$, equation A-6 can be written as,

$$\nabla^2 G(x,y) = \left(\frac{r^2 - 2\,\sigma^2}{\sigma^2} \right) \exp\left(\frac{-r^2}{2\,\sigma^2} \right) \qquad \text{A-7}$$

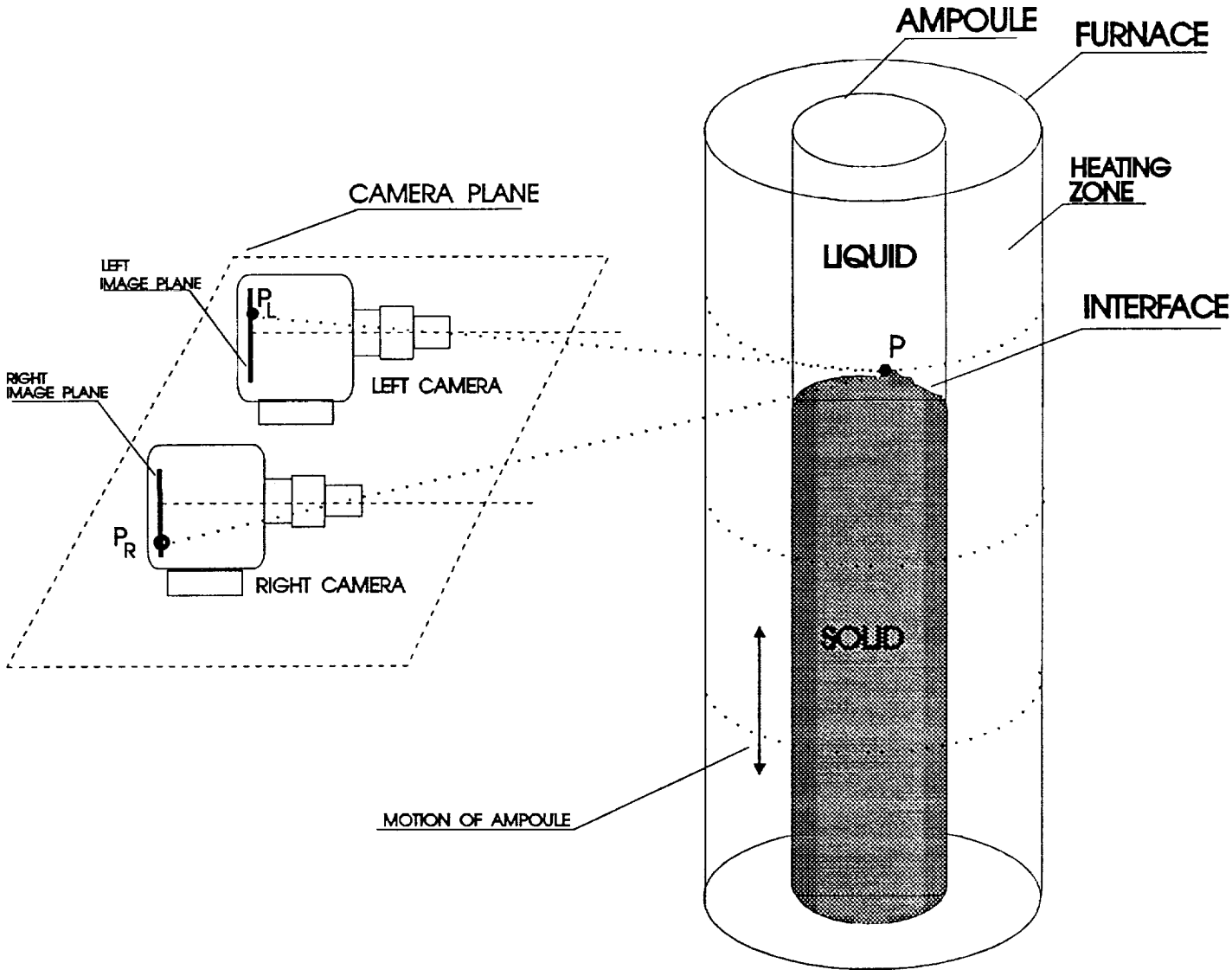

Figure 1. Stereo Imaging in a Transparent Furnace

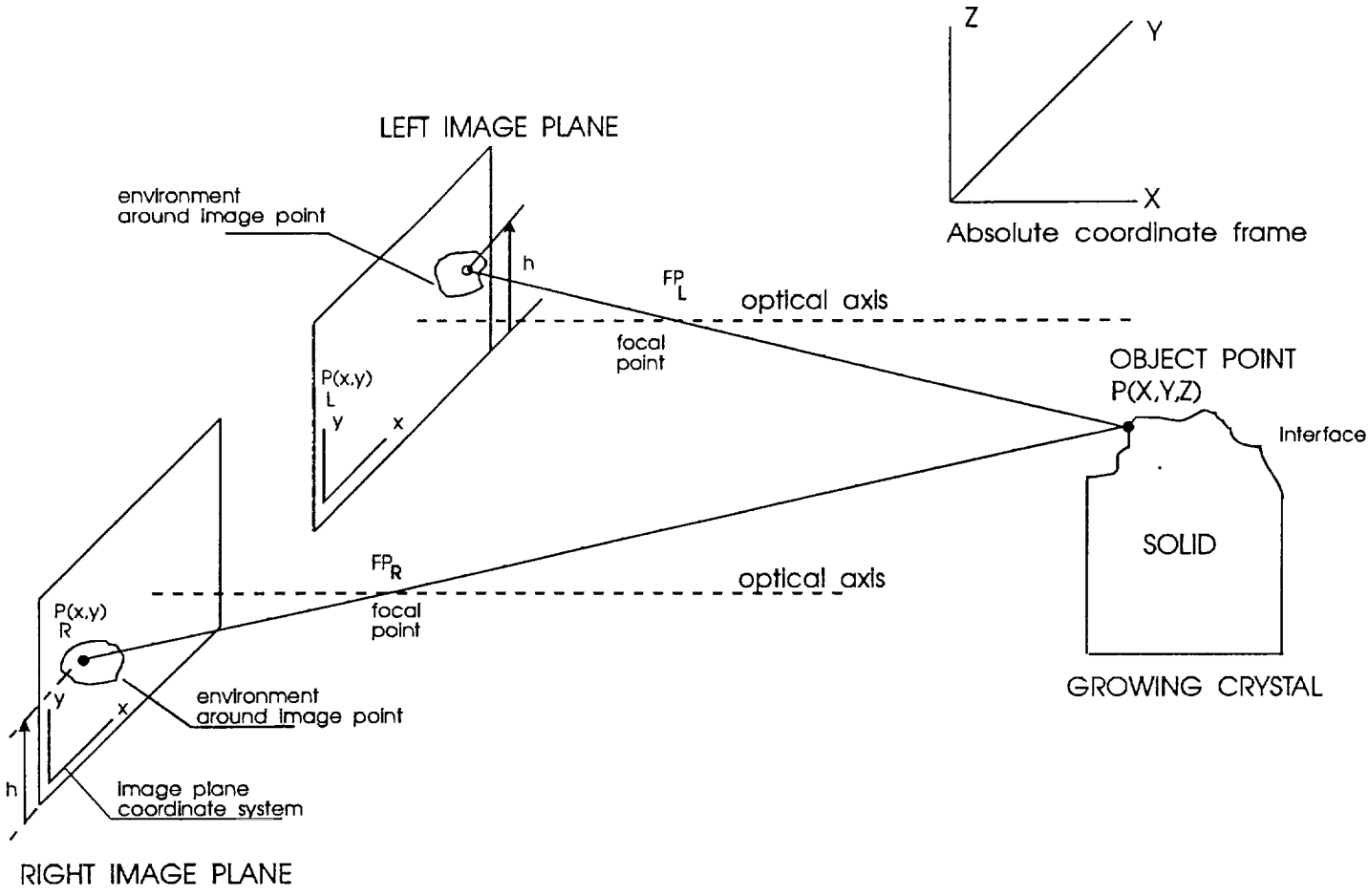

Figure 2. Stereo imaging of interface

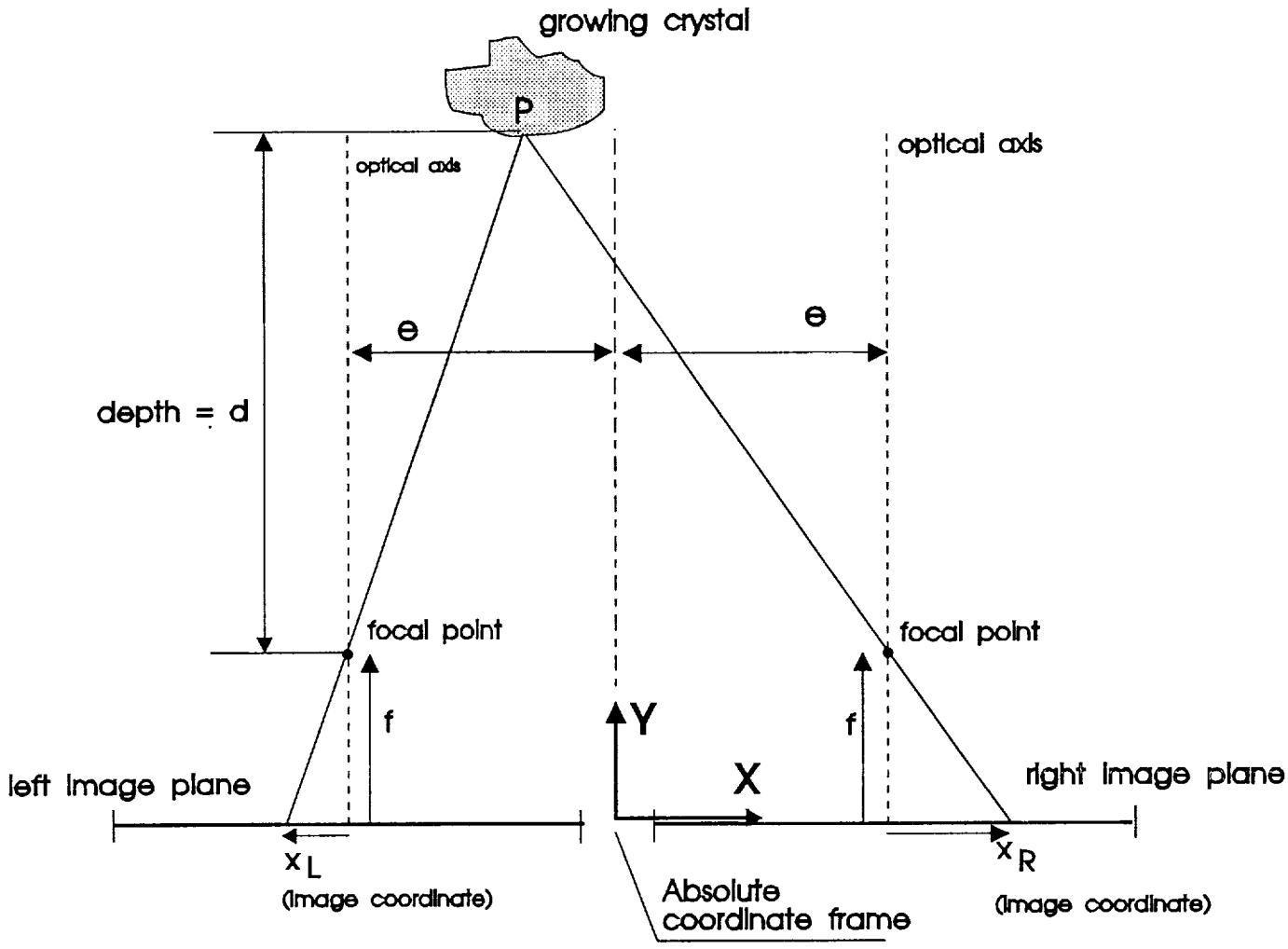

Figure 3. Determination of depth by stereo imaging

d=depth= $2.e.f / (x_R + x_L)$

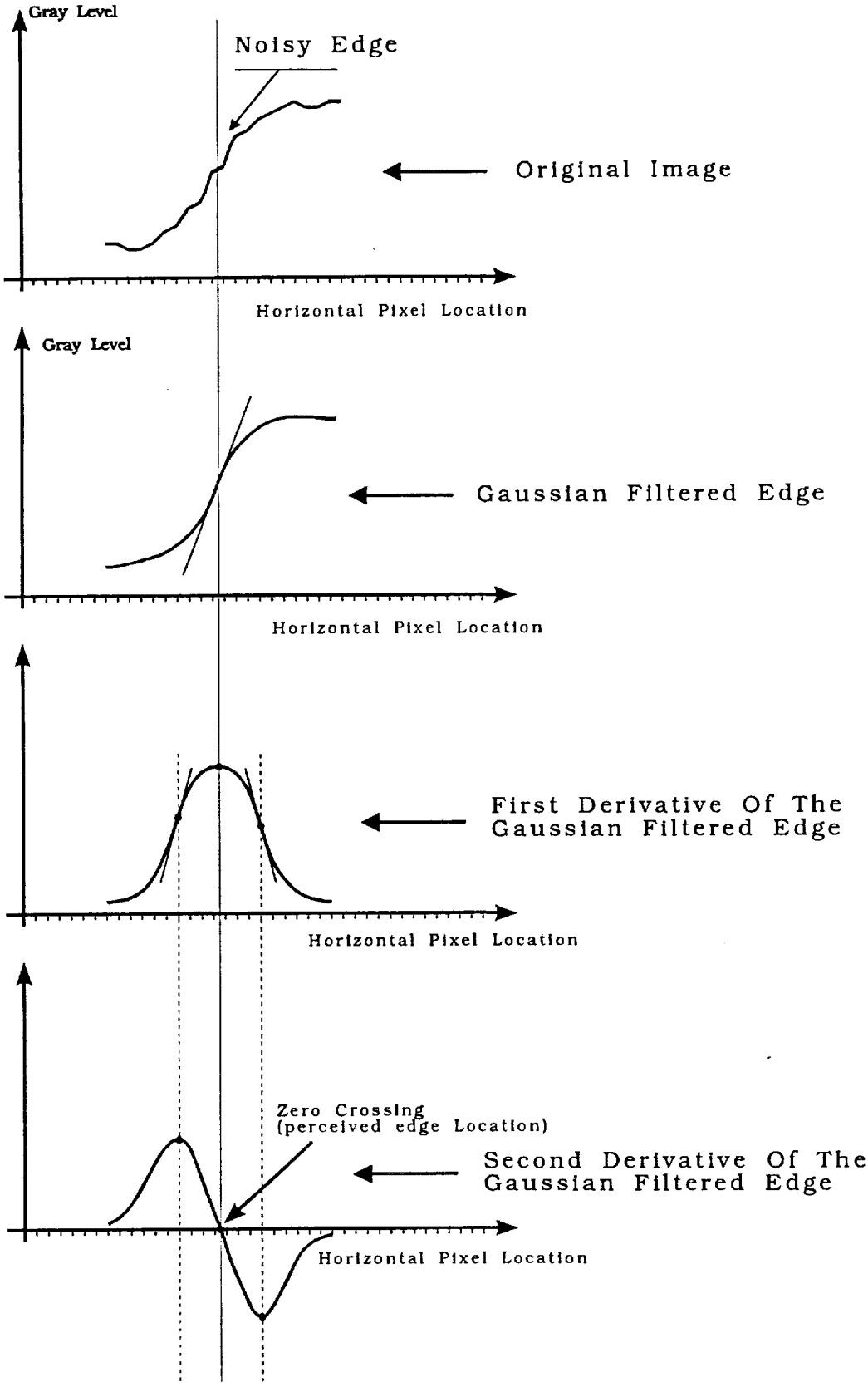

Figure 4. The effect of one dimensional LOG filter on a noisy edge

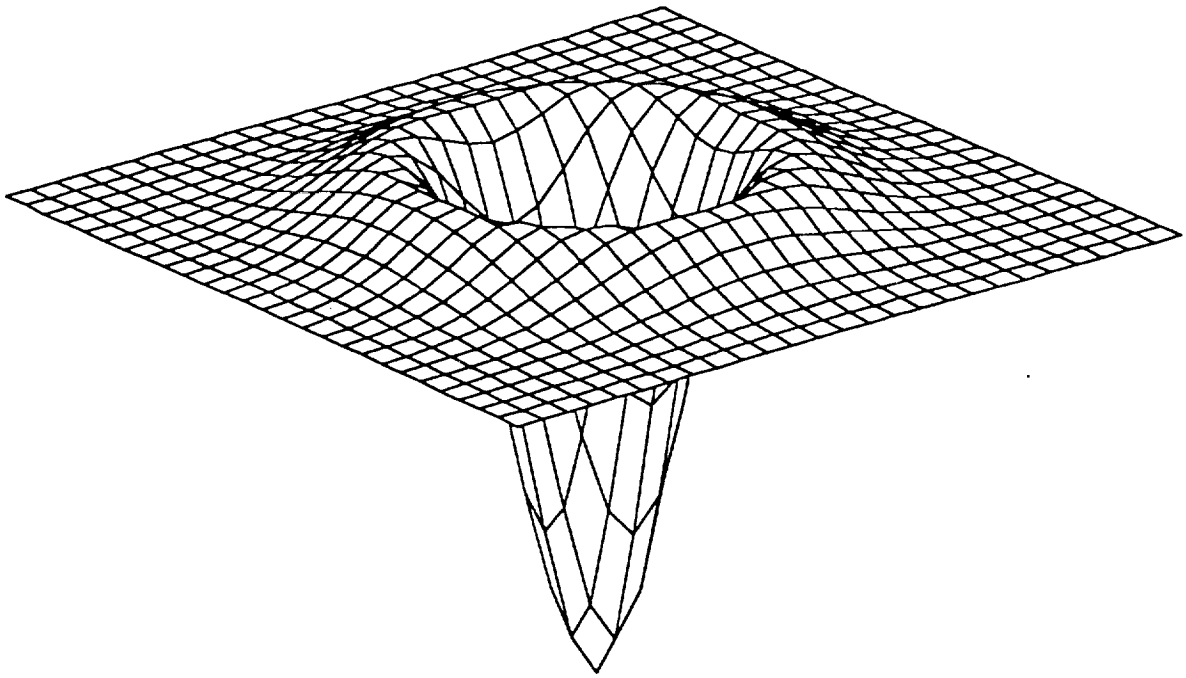

Figure 5. The shape of a typical LOG operator

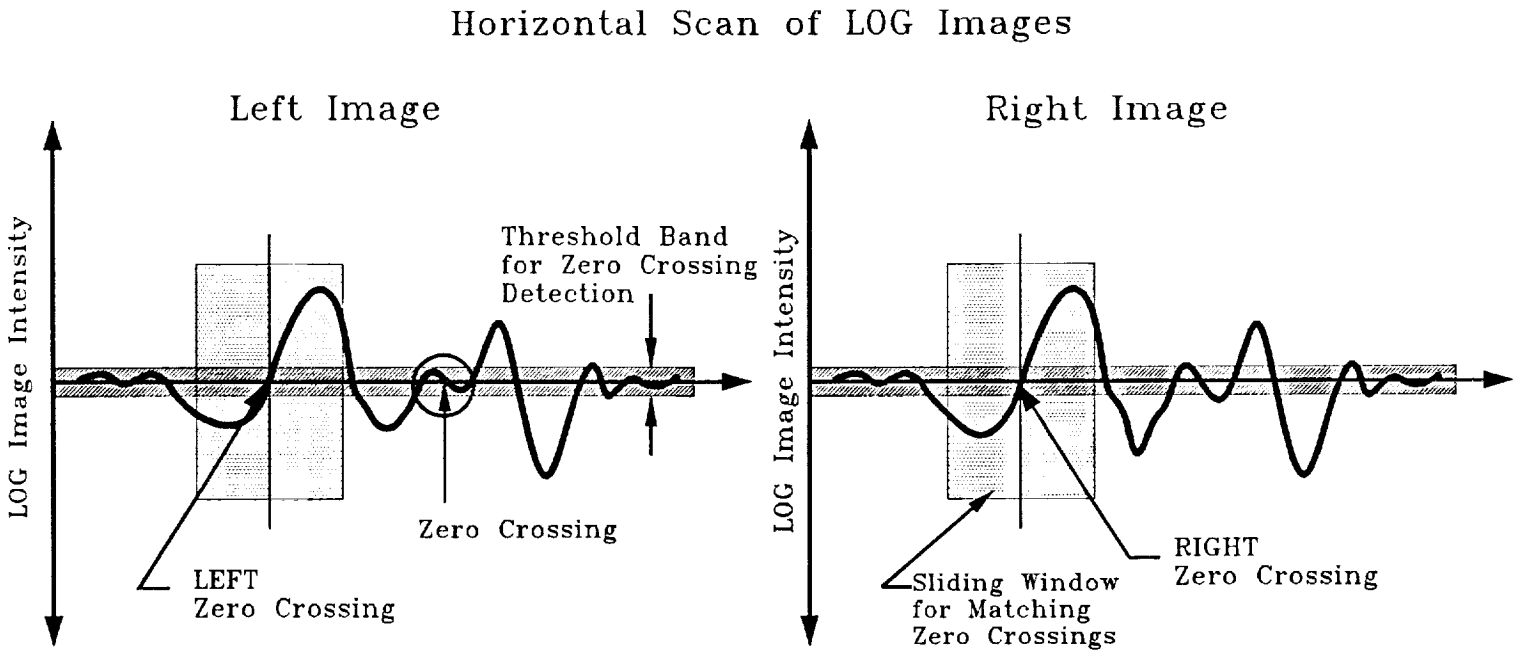

Figure 6. Illustration of matching procedure

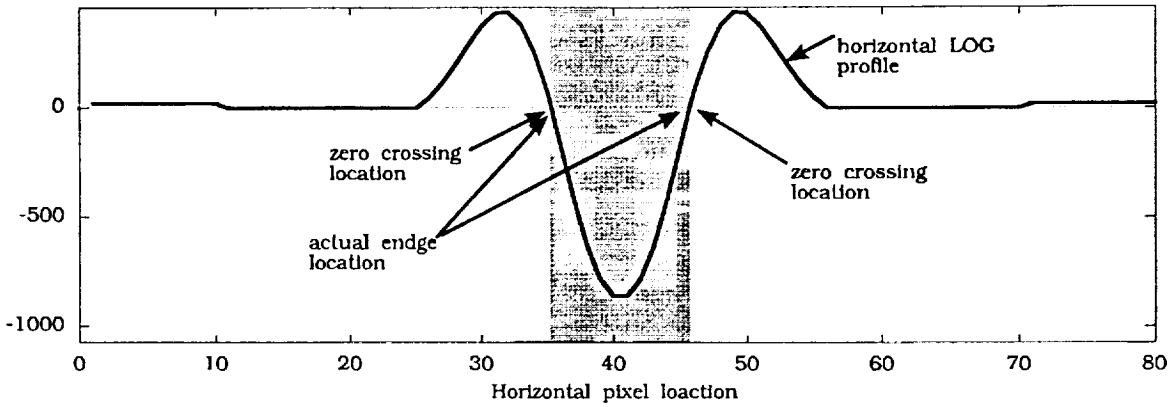

Figure 7a. Horizontal scan of LOG profile for the solid edge image (W_{2d}=11)

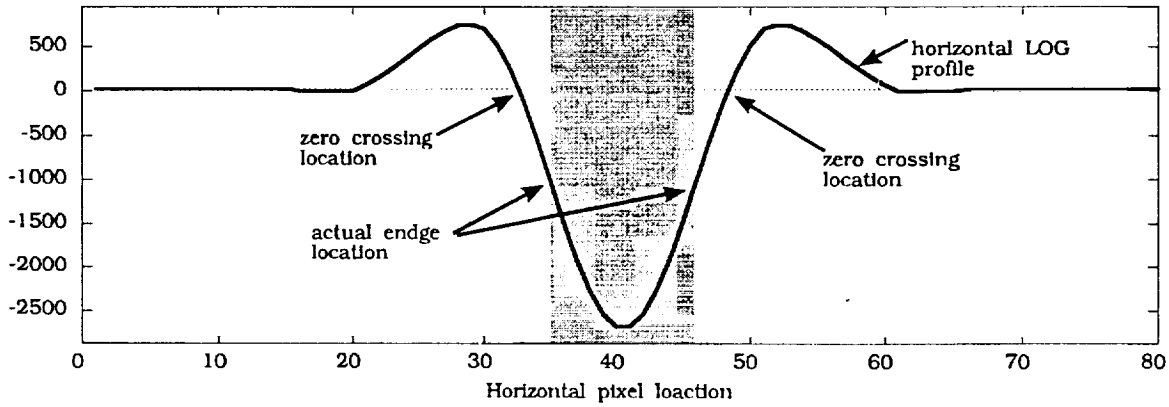

Figure 7b. Horizontal scan of LOG profile for the solid edge image (W_{2d}=17)

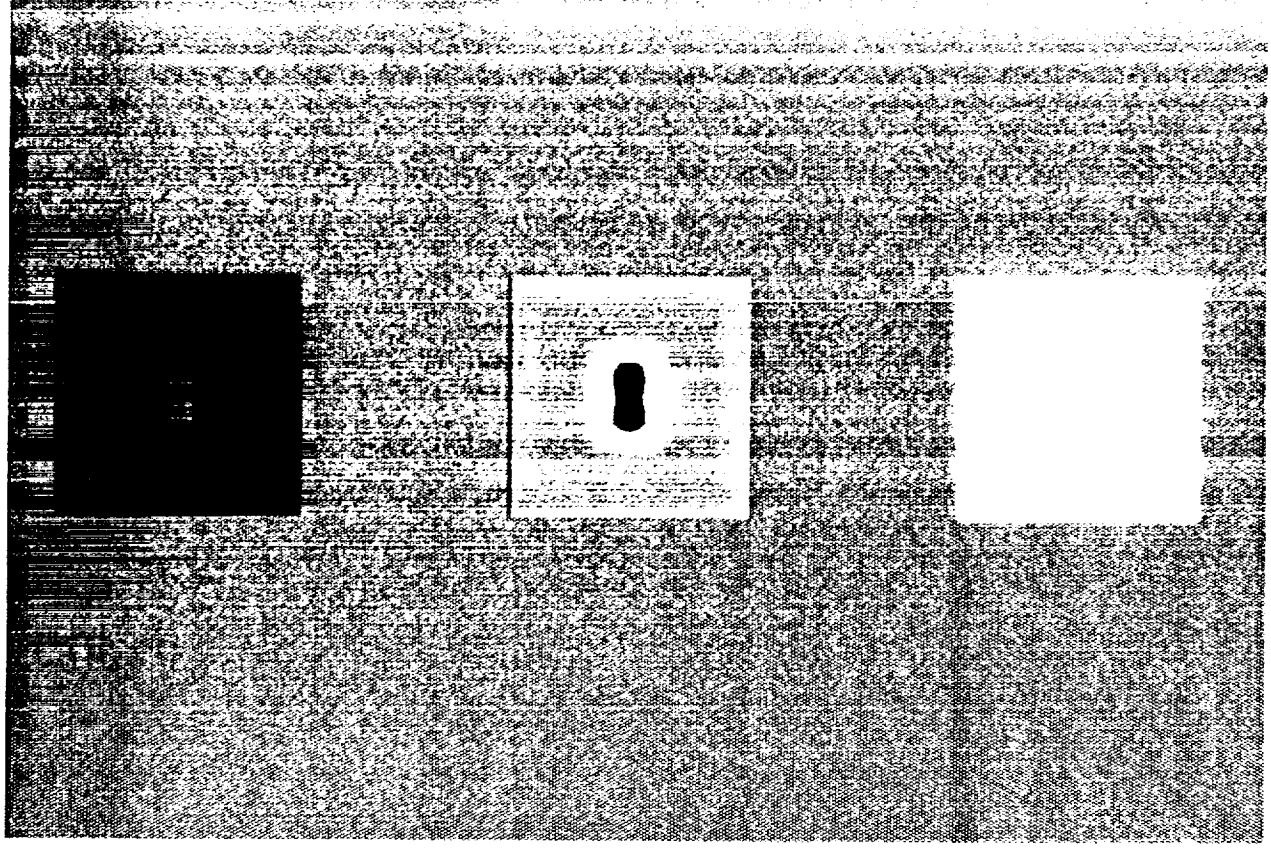

Figure 8a. Distortions in edge locations.
From left to right; original image, LOG image, zero crossing image (W_{2d}=11)

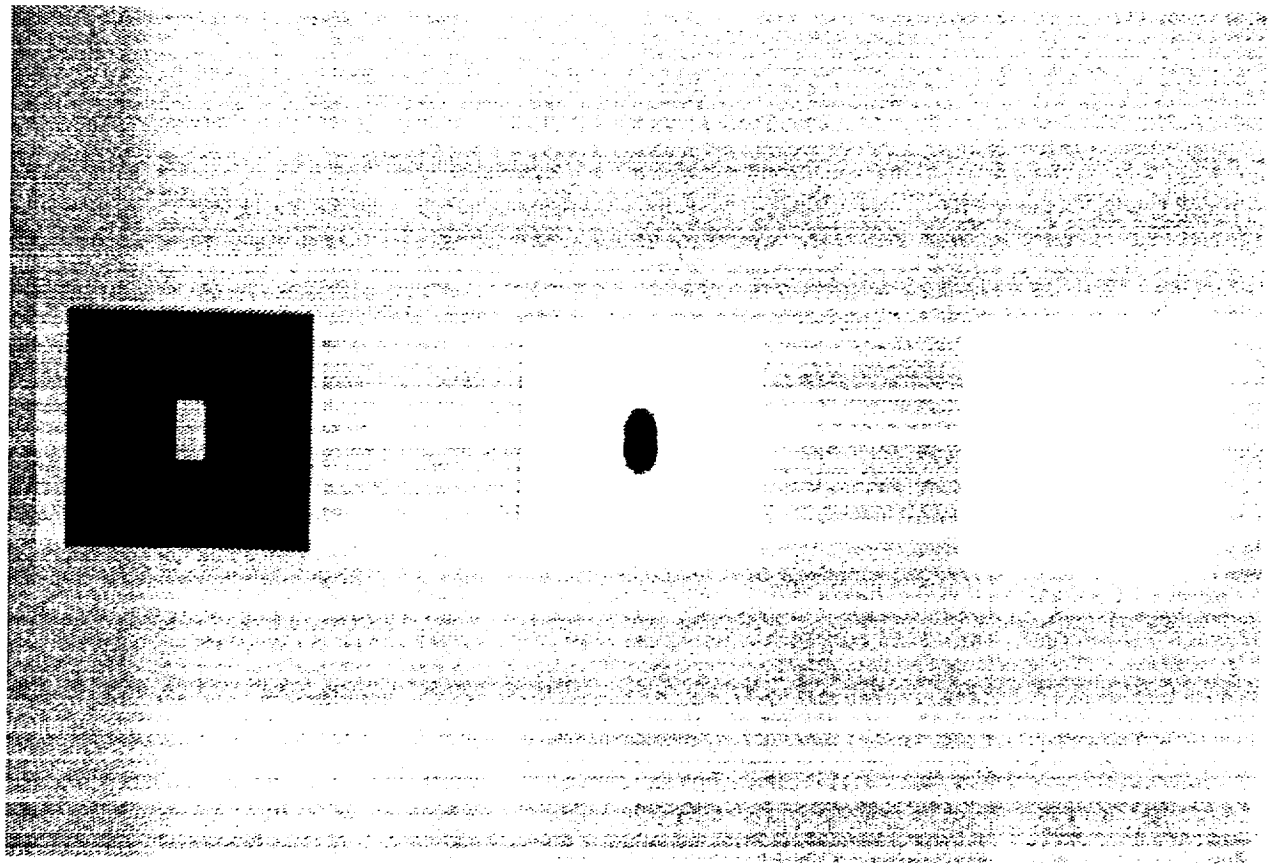

Figure. 8b. Distortions in edge locations.
From left to right; original image, LOG image, zero crossing image (W_{2d}=17)

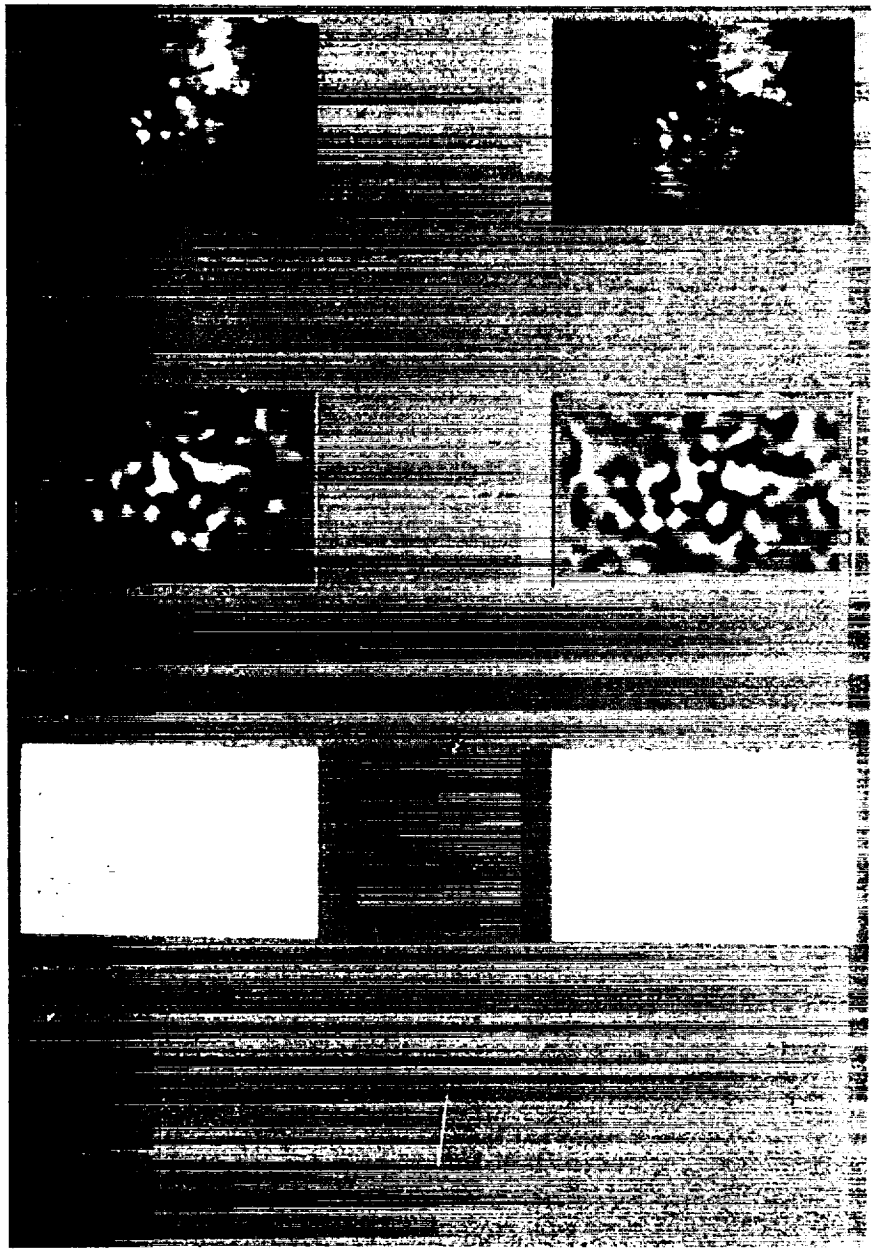

Figure 9 The original image, the LOG filtered image and the zero crossings from left and right cameras

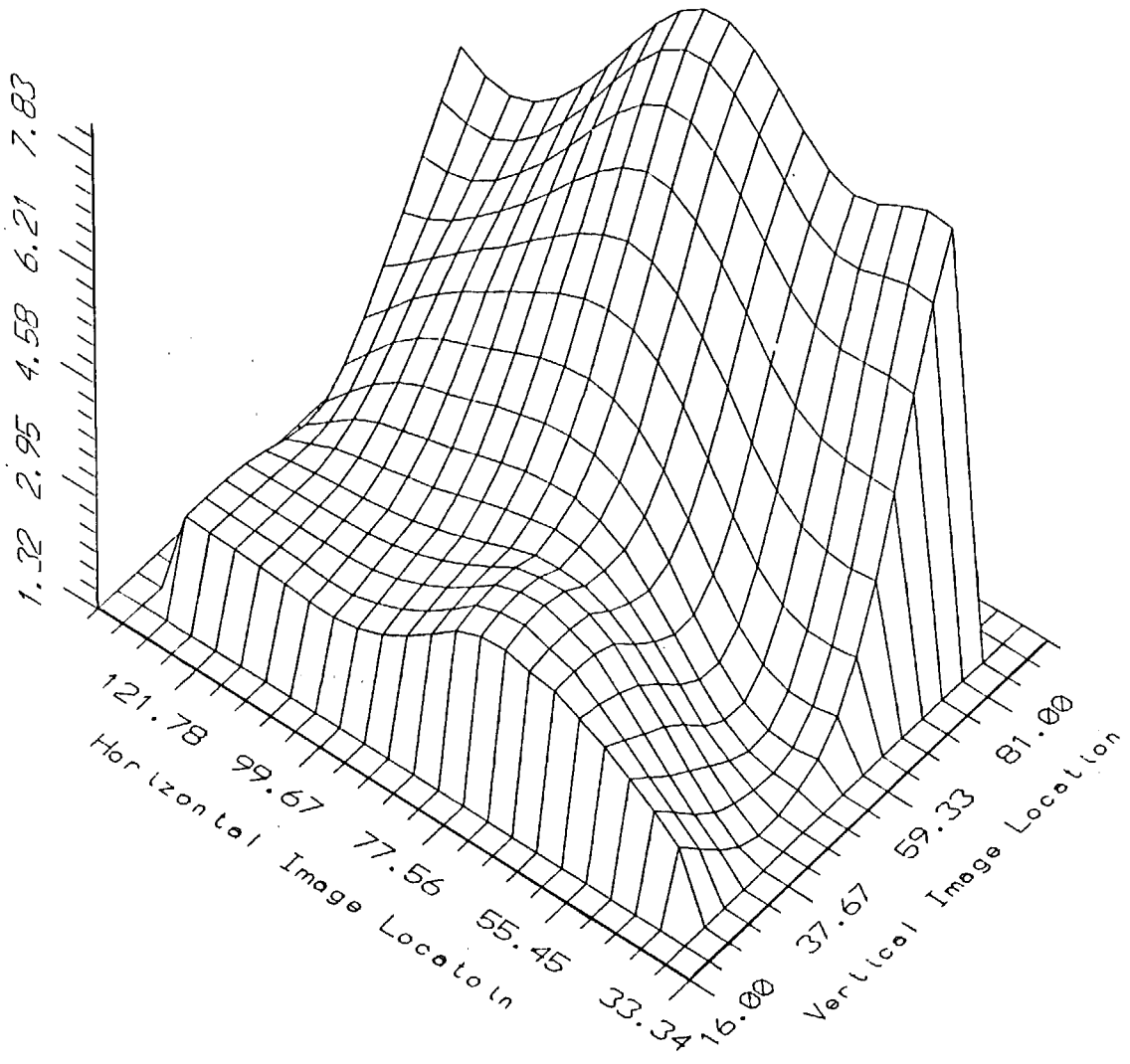

Figure 10a. Disparity profile for the images presented in Fig. 9

The left and right images are obtained from this region

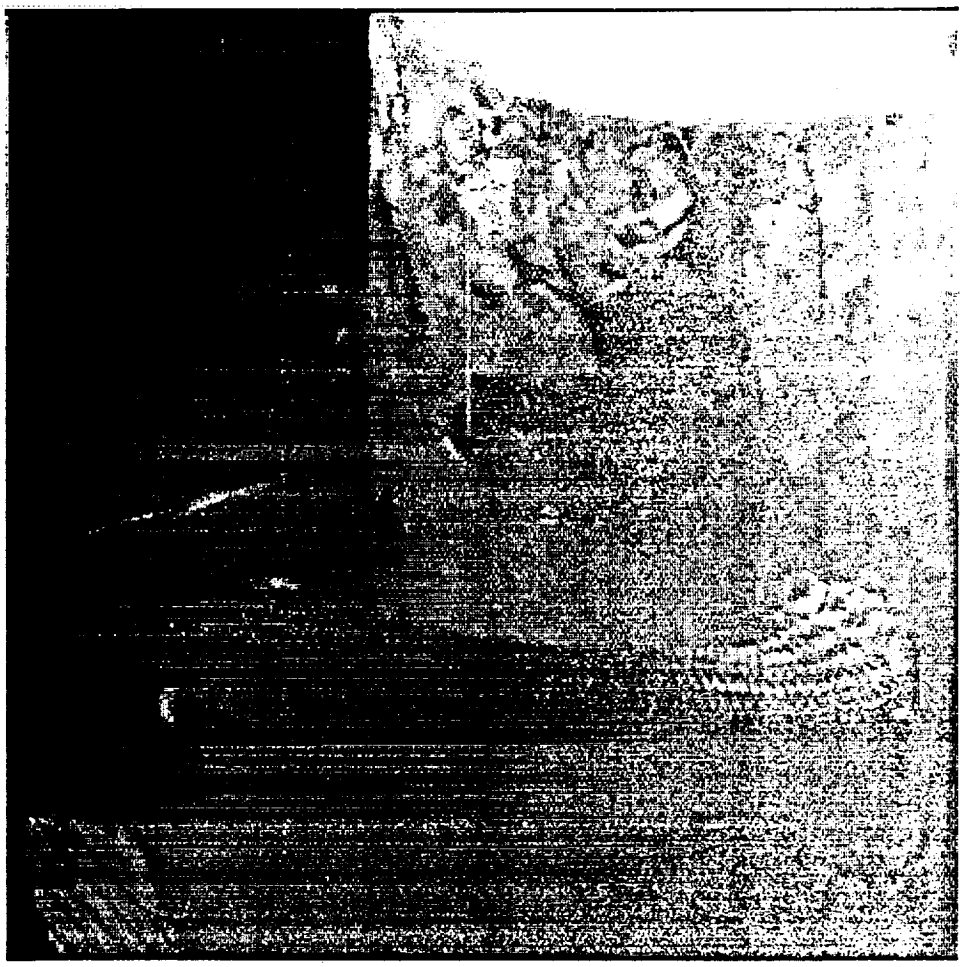

Figure 10b. A complete view of the crysytal inside the ampoule.
The section marked by the box is processed to determine the shape

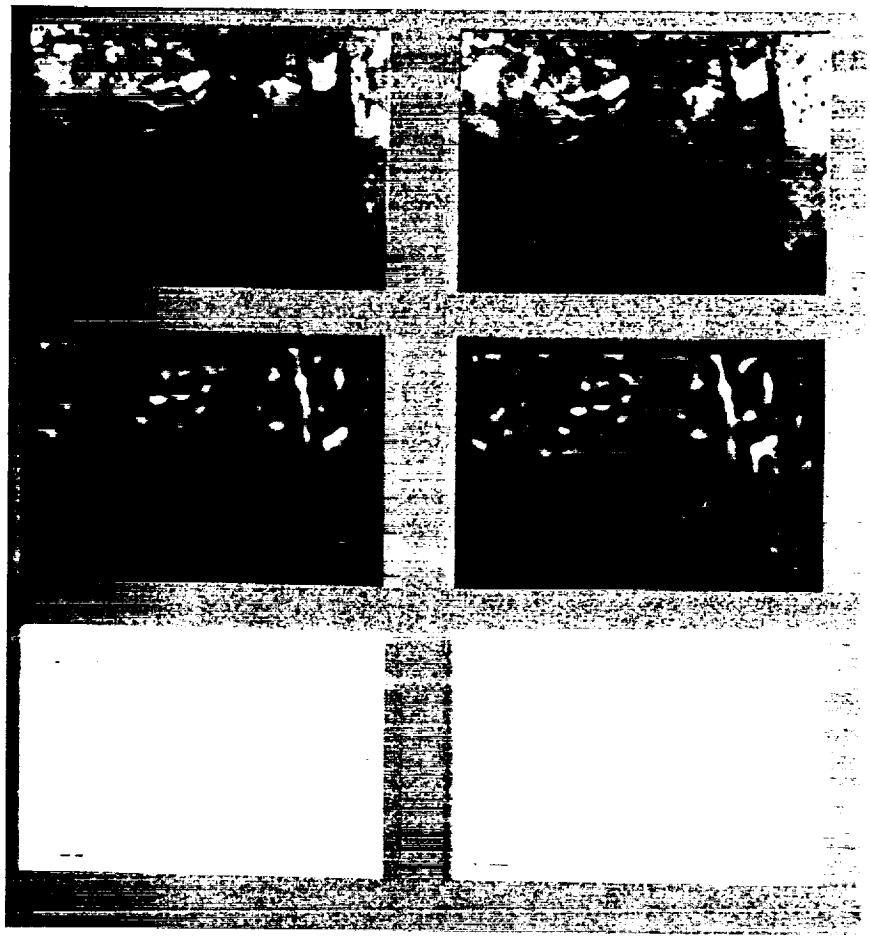

Figure 11 The original image, the LOG filtered image and the zero crossings from left and right cameras.

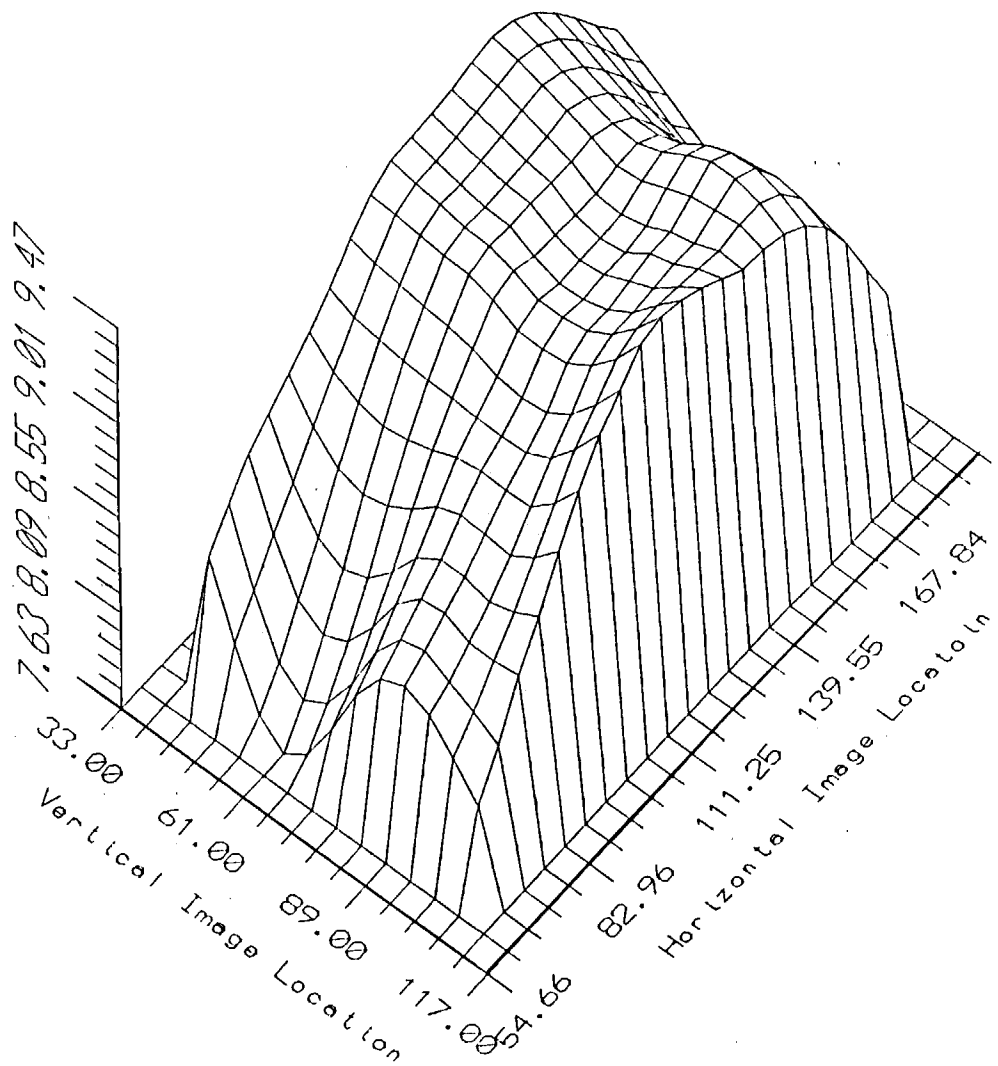

Figure 12. Disparity profile for the images presented in Fig. 11